

SIMULATION OF PHASED ARRAY WIDE-FIELD OF VIEW RADARS FOR SPACE SURVEILLANCE

J. Gelhaus¹, S. Flegel¹, C. Wiedemann¹, P.Vörsmann¹, S. Stabroth², A. Wagner², and H. Klinkrad³

¹Institute of Aerospace Systems, Technische Universität Braunschweig, Hermann Blenk Str. 23, 38108 Braunschweig

²EADS Astrium Satellites, 88039 Friedrichshafen, Germany

³Space Debris Office, ESA/ESOC, Robert-Bosch-Str. 5, 64293 Darmstadt

ABSTRACT

Europe intends to develop its own Space Surveillance System as part of a more comprehensive Space Situational Awareness System. In the design process, simulations help to determine appropriate system architectures for given user requirements. In order to provide such a simulation environment, the ESA Program for Radar and Optical Observation Forecasting (PROOF) can be applied. The existing model for phased-array radar simulations only takes into account a simplified antenna pattern. A new simulation approach is envisaged within a current PROOF software upgrade. It considers the complete scanning area as a single field-of-view, with borders of the scanning area defined relative to the line of sight, and with path offsets randomly selected to cover the scanning area.

Key words: PROOF; Space Surveillance; Radar; Phased Array.

1. INTRODUCTION

The ESA Program for Radar and Optical Observation Forecasting (PROOF) [1] is currently used for the validation of Debris Models (e.g. ESAs Meteoroid and Space Debris Terrestrial Environment Reference Model (MASTER)) (see [2]) and also for the planning of observation campaigns. The software can be split up into two main parts. In a first step a geometry filter computes all crossings of objects included in a user defined database. The position of the sensor and the objects are propagated to the observation epoch. Two different propagation approaches are used for the objects. In the statistical mode the MASTER reference population is used and the objects are propagated on undisturbed orbits. Only the right ascension of the ascending node (Ω) and the argument of the perigee (ω) are influenced by the Earth's gravity-field zonal harmonic term J_2 and propagated using Equation 1 and Equation 2. In the deterministic mode the object database is a user defined number of Two-Line-elements (TLEs). These objects are propagated us-

ing the Simplified General Perturbations Satellite Orbit Model (SGP4/SDP4) algorithms. The timesteps for the propagation depend on the offset angle the object has to the line of sight (LOS) of the user defined field of view (FOV) in combination with the distance to the line of sight.

$$\Delta\Omega_{day} = -9.96^\circ \cdot \frac{\left(\frac{R_E}{a}\right)^{\frac{7}{2}} \cdot (\cos i)}{(1 - \epsilon^2)^2} \quad (1)$$

$$\Delta\omega_{day} = 4.98^\circ \cdot \frac{\left(\frac{R_E}{a}\right)^2 \cdot (5 \cdot \cos^2 i - 1)}{(1 - \epsilon^2)^2} \quad (2)$$

with

R_E	=	Mean radius of Earth
	=	6371.00877 [km]
a	=	Semi-major axis of object orbit
i	=	Inclination of object orbit
ϵ	=	Eccentricity of object orbit

After the crossing analysis is made these crossings are analysis with one of the two performance models. For telescopes an optical performance model comprises the properties of the object (size, shape, total reflectance of the surface) in combination with a night sky model which considers the background radiation. For radar the radar performance model is generating the detection probability for all crossing objects with respect to the object range, velocity and radar cross section. Finally detection rates are provided to the user.

To simulate sensor systems as they are used in space surveillance systems this performance was extended to generate pseudo measurements based on the crossing geometry of all detected objects. [3]

2. PSEUDO MEASUREMENTS

The generation of pseudo measurements is based on the existing performance of PROOF as described in Section 1. The generated output files for the pseudo measurements will include azimuth and elevation or right ascension and

declination of the object for both types of sensors and a range and range rate information if the sensor is a radar. Also the time of each measurement will be provided as well as the sensor position at this time. For bistatic radars the output will include two sensor positions. One for the transmitter site and another for the receiver site. In any radar case the range information is the two way range from the transmitter to the object and down to the receiver.

The geometry of the crossing object is described in a cone fixed coordinate system (CONE) of the sensor inside the geometry filter. To use this data for generating the pseudo measurements the object status vector has to be transformed into the earth centered inertial coordinate system (ECI).

2.1. Transformation between CONE and ECI

The CONE coordinate system is fixed to the sensor line of sight. The x-axis is in line with the sensor line of sight while the z-axis is pointing north and the y-axis completes the coordinate system as it is a right hand system. For the geometry analysis and the crossing decision the object state vector \vec{y} in the ECI coordinate system is transformed into the CONE system. Therefore the vector \vec{y}_{ECI} is multiplied with the transformation matrix M as defined in Equation 3 in combination with the Equations 4 - 6. The right ascension α and declination δ of the line of sight has to be known.

$$\vec{y}_{CONE} = M[\vec{M}_1, \vec{M}_2, \vec{M}_3] \cdot \vec{y}_{ECI} \quad (3)$$

with

$$\vec{M}_1 = \begin{pmatrix} \cos(\alpha) \cos(\delta) \\ \cos(\alpha) \sin(\delta) \\ -\sin(\alpha) \end{pmatrix} \quad (4)$$

$$\vec{M}_2 = \begin{pmatrix} \sin(\alpha) \cos(\delta) \\ \sin(\alpha) \sin(\delta) \\ \cos(\alpha) \end{pmatrix} \quad (5)$$

$$\vec{M}_3 = \begin{pmatrix} \sin(\delta) \\ -\cos(\delta) \\ 0 \end{pmatrix} \quad (6)$$

After the geometry analysis the transformed object state vector \vec{y}_{CONE} is available and has to be transformed back into the ECI coordinate system. This vector has to be used instead of the original object state in the ECI coordinate system, because the atmospheric refraction that has a influence on the elevation angle was added to the \vec{y}_{CONE} during the geometry analysis. For this transformation the inverse matrix M^{-1} has to be created and multiplied with the object state \vec{y} given in the CONE coordinate system as defined in Equation 7 in combination with the Equations 8 - 10.

$$\vec{y}_{ECI} = M^{-1}[\vec{M}_1^{-1}, \vec{M}_2^{-1}, \vec{M}_3^{-1}] \cdot \vec{y}_{CONE} \quad (7)$$

with

$$\vec{M}_1^{-1} = \begin{pmatrix} \cos(\alpha) \cos(\delta) \\ \sin(\alpha) \cos(\delta) \\ \sin(\delta) \end{pmatrix} \quad (8)$$

$$\vec{M}_2^{-1} = \begin{pmatrix} \cos(\alpha) \sin(\delta) \\ \sin(\alpha) \sin(\delta) \\ -\cos(\delta) \end{pmatrix} \quad (9)$$

$$\vec{M}_3^{-1} = \begin{pmatrix} -\sin(\alpha) \\ \cos(\alpha) \\ 0 \end{pmatrix} \quad (10)$$

2.2. Generation of Pseudo Measurements

To compute the direction angles as azimuth and elevation the ECI object state has to be transformed into the local horizon system (LH) of the sensor. Either the local horizon system is the one of the optical sensor or the monostatic radar or it is the one of the receiver (RC) in case of bistatic radars. Because the x-axis is pointing north and the z-axis is pointing into the zenith the azimuth A has to be generated with Equation 11. The elevation h can be generated with Equation 12.

$$A = \arctan\left(\frac{-y_{LH}}{x_{LH}}\right) \quad (11)$$

$$h = \arcsin\left(\frac{z_{LH}}{\sqrt{x_{LH}^2 + y_{LH}^2 + z_{LH}^2}}\right) \quad (12)$$

The right ascension α and declination δ can be calculated without a transformation of the object state into the local horizon system with Equation 13 and 14.

$$\alpha = \arctan\left(\frac{y_{ECI}}{x_{ECI}}\right) \quad (13)$$

$$\delta = \arcsin\left(\frac{z_{ECI}}{\sqrt{x_{ECI}^2 + y_{ECI}^2 + z_{ECI}^2}}\right) \quad (14)$$

This already includes the calculation of the one-way range. The two-way range r as it can be computed by using the run time of a signal in real systems is calculated by using both the information of the object position in the transmitter system (TR) and in the receiver system (RC).

$$r = \sqrt{x_{ECI,TR}^2 + y_{ECI,TR}^2 + z_{ECI,TR}^2} + \sqrt{x_{ECI,RC}^2 + y_{ECI,RC}^2 + z_{ECI,RC}^2} \quad (15)$$

The range-rate \dot{r} is calculated by using two consecutive range informations and the time t of these two steps

$$\dot{r} = \frac{r_{t_1} - r_{t_2}}{t_1 - t_2} \quad (16)$$

In Equation 15 and Equation 16 the object state in the ECI system is used. The result will be the same using the LH coordinates.

Because in real systems bias, noise and maybe a drift are included in the measurements these values can be defined for all four measurement types (direction angles, range and range-rate). Since an atmospheric model is already included in PROOF these values are sensor specific

caused by the component itself and changed over time by their age. The noise has to be defined as peak-to-peak value n . After a randomized selection of a noise level this value is added together with the bias to the pure measurement data.

$$r = r_{pure} + r_{bias} + r_{noise} + r_{drift} \quad (17)$$

with

$$r_{noise} \in \left[-\frac{n}{2}, +\frac{n}{2} \right]$$

2.3. Measurement results of a modeled Phased Array

In the last PROOF version there is already a phased array mode included. This mode takes into account that the line of sight may have an offset to the phased array normal direction (PAND) and is restricted to the radar performance model. To consider also the scanning area of a

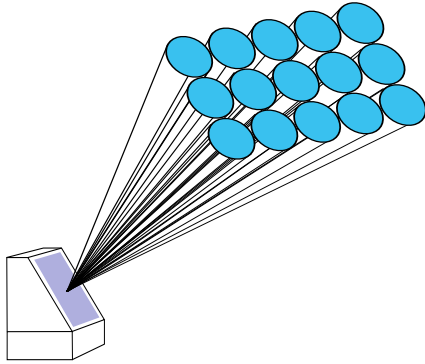


Figure 1. Phased Array simulation with PROOF-2005

phased array the automatic mode of PROOF can be used. This mode allows the user to define e.g. different fields of view orientations (see Figure 1). A large number of fields of view has to be defined to cover the scanning area of a phased arrays. As Figure 1 shows there are gaps between the single fields of view due to their circular shape. Using this formation will cause also gaps in the generated measurements as shown in Figure 2. If an object is not detectable in a single FOV these gaps can be even larger than the normal gap due to the not covered space between the circular fields of view. Since the timesteps for the object propagation inside the field of view is computed using the field of view dwell time the timesteps between the generated measurements are also different for every single field of view.

A rough estimation for the simulation of the scanning area (180° azimuth x 20° elevation) of the GRAVES system with an assumed field of view of two degree leads to 900 single fields of view. The number of single fields of view is equal to the number of PROOF runs. This results in long run times for the simulation of phased arrays in

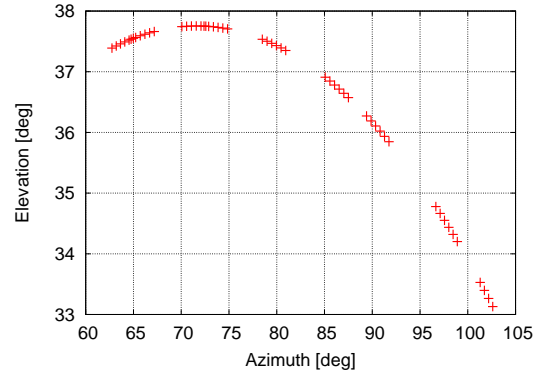


Figure 2. Azimuth and elevation distribution with gaps between single FOVs for a single object crossing the synthesized large field of view

the context of space surveillance where often also a large number of objects is analyzed.

To decrease these long run times an additional and more user-friendly model for the phased array simulation will be developed and implemented in the next PROOF version.

3. AN ADDITIONAL MODEL FOR THE PHASED ARRAY SIMULATION

A new model for the simulation of phased arrays is needed to increase the performance of PROOF for this task. Synthesizing a large scanning area by a large number of individual fields of view is no longer useful for the use of PROOF in the context of space surveillance. The approach is to define a large field of view (called 'scanning area' in the following) for the geometry filter by using the still defined line of sight as centre of this scanning area. Figure 3 shows the scanning area of a phased array using this new approach with a line of sight in line with the phased array normal direction. Two additional parameters have to be defined by the user. The difference in azimuth/right ascension ($\Delta A/\Delta \alpha$) and in elevation/declination ($\Delta h/\Delta \delta$) from the center to the borders of the scanning area as shown in Figure 3.

In this approach the circular field of view as defined by the user is only used for the detection analysis. Since there is no circular field of view in the new geometrical approach the generation of the timesteps for object propagation has to be changed. The present approach uses the offset angle between the line of sight and the object state vector together with the perpendicular distance between object and line of sight. With lower distance the timesteps for propagation decrease. For objects crossing the field of view the point of closest approach to the line of sight (the point, where the timesteps are the smallest) is always inside the field of view. For a rectangular scanning area in the additional model the point of closest approach

is not mandatory inside. Crossing objects will possibly not be detected using the present propagation method if their crossing occurs far-off the line of sight where the timesteps are to large. Therefore a new method was developed to generate the timesteps for object propagation.

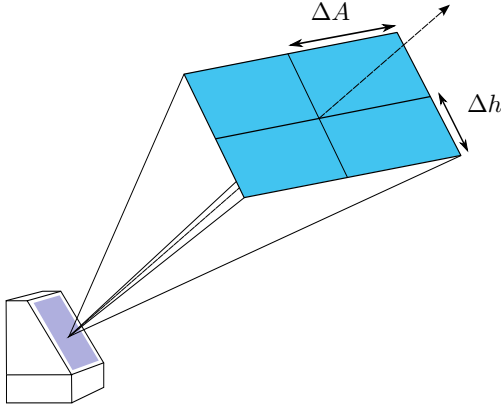


Figure 3. Envisaged phased array simulation

3.1. Modification in the Geometry Filter

Instead of the offset angle wrt. the line of sight the new method computes the offset angle wrt. the border of the scanning area as long as the object is outside the scanning area. For this computation spherical trigonometry is used although the explanation in Figure 4 is made with Euclidean geometry (NOTE: $\alpha \neq \beta$).

First it is assumed that the object is outside the scanning area (dashed line) with the angular distance ΔA and Δh normal to the line of sight. The angle γ as defined in Figure 4 is

$$\gamma = \arctan\left(\frac{\tan(\Delta A_{obj})}{\sin(\Delta h_{obj})}\right) \quad (18)$$

and has to be smaller than

$$\gamma_{max} = \arctan\left(\frac{\tan(\Delta A_{SA})}{\sin(\Delta h_{SA})}\right) \quad (19)$$

for the use of the following equations. The direct angular distance δ_{obj} to the line of sight is

$$\delta_{obj} = \arccos(\cos(\Delta A_{obj}) \cdot \cos(\Delta h_{obj})) \quad (20)$$

while the direct angular distance δ_{SA} from the line of sight to the border of the scanning area is

$$\delta_{SA} = \arctan\left(\frac{\tan(\Delta h_{SA})}{\cos(\gamma)}\right) \quad (21)$$

With Equation 20 and 21 the angular distance from the object to the scanning area in the direction of the line of sight can be computed (Equation 22).

$$\delta_{offset} = \delta_{obj} - \delta_{SA} \quad (22)$$

This leads to a distance of

$$r_{offset} = \frac{\pi \cdot r}{180^\circ} \cdot \delta_{offset} \quad (23)$$

with r as range between object and sensor. At this point a fictional field of view with a four times large diameter than defined for the field of view used in the detection analysis is assumed at the border of the scanning area where the direct angular distance δ_{obj} is crossing and the old methods for generating the timesteps is used with the new determined r_{offset} . This fictional field of view is replaced at the border of the scanning area for every timestep. As long as the offset angle δ_{offset} is larger than $2 \cdot FOV$ the timestep for the next propagation step during the simulation Δt_{sim} is chosen by

$$\Delta t_{sim} = \frac{r_{offset}}{15 \frac{km}{s}} \quad (24)$$

For offset angles smaller than $2 \cdot FOV$ the timestep is

$$\Delta t_{sim} = \frac{r_{offset} - 0.99 \cdot \tan\left(\frac{FOV}{2}\right) \cdot r_{obj}}{50 \frac{km}{s}} \quad (25)$$

If the object finally is inside the scanning area the timesteps for propagation are determined. Therefore, the object is propagated forward and backward in time to find the access time t_1 and the exit time t_2 . The timestep is then computed as

$$\Delta t_{sim} = \frac{t_2 - t_1}{N_{sim}} \quad (26)$$

with N_{sim} as the number of timesteps inside the scanning area. With this timestep the crossing geometry is generated.

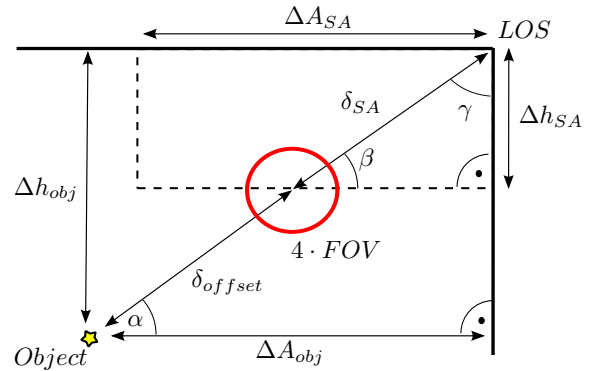


Figure 4. Object propagation for a rectangular scanning area (one quarter)

The expected results for the measurement generation using the changed geometry filter are shown in Figure 5. Gaps between the measurements should no longer exist so that the complete path of the object while it is inside the scanning area is reflected.

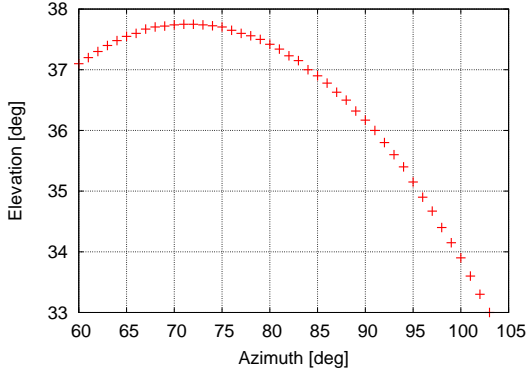


Figure 5. Envisaged distribution of measurements (here with a constant azimuth steps)

3.2. Modification in the Detection Filter

After the modifications in the geometry filter have been described the required modifications of the subsequent filter for the detection analysis will be explained.

The first modification is the determination of the crossing point that will be analyzed. Using the present method the point of closest approach wrt. the line of sight is analysed for detectability. At this point the possibility for a successful detection is the largest. Using the new approach for scanning areas the point of closest approach wrt. the line of sight is the point with the largest detection possibility iff the line of sight is in line with the phased array normal direction. If the line of sight as pointer for the center of the scanning area is far away from the phased array normal direction the objects close to the line of sight may not be detectable while the object during the crossing is detectable at a point closest to the phased array normal direction. For this reason the detection analysis is made for for the point closest to the phased array normal direction.

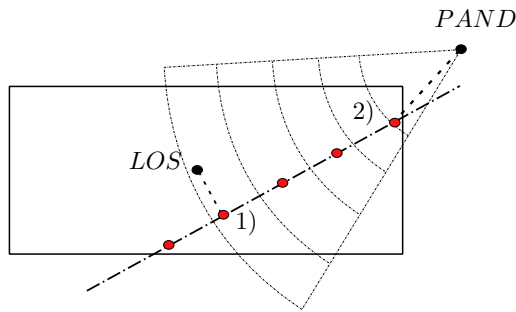


Figure 6. The Points of closest approach: 1) to the line of sight; 2) to the phased array normal direction

The second modification is caused by the fact that the path offset can not be determined as done in the present approach. The path offset is the distance perpendicular to the path and pointing towards the line of sight. Since the movement of the beam over the scanning area is not com-

puted in detail the path offset will be randomly selected between 0 and the 3dB beamwidth.

A third modification is made for the determination of the number of pulses to integrate. There the user has to define the scanning period T_{scan} . This is the time the beam needs to move completely over the scanning area and back to the starting point for one cycle. Also the coverage R_{cov} of the scanning area by the beam is computed. This is the ratio of the defined FOV of the moving beam and the scanning area and can be defined as

$$R_{cov} = \frac{FOV^2}{\Delta A_{SA} \cdot \Delta h_{SA}} \quad (27)$$

Finally, the Number of pulses to integrate N is a function of the scanning period T_{scan} , the coverage of the scanning area by the FOV (of the transmitter) R_{cov} and the pulse repetition period T_{pr} defined by the user.

$$N = f(T_{scan}, R_{cov}, T_{pr}) \quad (28)$$

4. CONCLUSION

In this paper two new extension of the software PROOF for the use in the context of space surveillance have been discussed. At first it has been shown that PROOF can be used for the generation of measurements of a space surveillance sensor. This enables PROOF to simulate a complete sensor with the object and sensor propagation to extract the crossing objects out of a given database, with a subsequent detection analysis to extract the detected objects out of the crossings and finally with the measurement generation for all detected objects. As PROOF was used for this task it becomes clear that the simulation of phased arrays has to be retrieved due to a complex definition of the scanning area synthesized by a large number of individual fields of view and even more due to the long run times caused by the large number of individual fields of view where each is representing a single PROOF run. This leads to a new model of phased array simulation described in the second part of this chapter. The scanning area of a phased array is specified by two dimensions in orthogonal directions to the line of sight. A new propagation procedure has been developed to decrease the simulated timesteps for objects coming closer to the border of the scanning area. Also the detection analysis was modified to take into account that the beam is not fixed but moving to cover the complete scanning area with a defined scanning period.

The next PROOF version is currently developed under ESA contract and will contain the new model for the phased array simulation. The generation of measurements was developed during an ESA contract in context of space surveillance and will not be available to the populace of users in the next PROOF version.

ACKNOWLEDGMENTS

The work presented in this paper was achieved during the ESA studies “Proof of Concept for Enabling Technologies for Space Surveillance” (first part) and “Maintenance of the MASTER model” (second part). All responsibilities for the contents of this publication reside with the authors.

REFERENCES

- [1] Oswald M., Wiedemann C., Krag H., Rosebrock J., Schildknecht T., PROOF - Final Report, Institute of Aerospace Systems, Technische Universität Braunschweig, European Space Agency, Contract: 18014/03/D/HK (SC), Document ID: M05/GEN-WP5000, Rev. 1.1, April 27, 2006
- [2] Oswald M., Stabroth S., Wiedemann C., Wegener P., Martin C., Upgrade of the MASTER Model - Final Report, Institute of Aerospace Systems, Technische Universität Braunschweig, European Space Agency, Contract: 18014/03/D/HK (SC), Document ID: M05/MAS-FR, Rev. 1.0, April 26, 2006
- [3] Simulation of sensor specific measurement data for orbit determination of satellites, Institute of Aerospace Systems, Technische Universität Braunschweig, Document ID: R-0721 D, April 08, 2008